Available online at www.sciencedirect.com
SCIENCE DIRECT®
International Journal of Solids and Structures 43 (2006) 982–1008
INTERNATIONAL JOURNAL OF SOLIDS and STRUCTURES
www.elsevier.com/locate/ijsolstr

Acoustical characterization of fluid-saturated porous media with local heterogeneities: Theory and application

Changfu Wei [a], Kanthasamy K. Muraleetharan [b,*]

[a] *Department of Civil Engineering, University of Vermont, 33 Colchester Avenue, 213 Votey Building, Burlington, VT 05401, USA*
[b] *School of Civil Engineering and Environmental Science, University of Oklahoma, 202 W. Boyd Street, Room 334, Norman, OK 73019, USA*

Received 22 October 2004; received in revised form 2 June 2005
Available online 20 July 2005

Abstract

A linear dynamic model of fully saturated porous media with local (either microscopic or mesoscopic) heterogeneities is developed within the context of Biot's theory of poroelasticity. Viscoporoelastic behavior associated with local fluid flow is characterized by the notion of the dynamic compatibility condition on the interface between the solid and the fluid. Complex, frequency-dependent material parameters characterizing the viscoporoelasticity are derived. The complex properties can be obtained through determining the quasi-static poroelastic parameters, the properties of individual constituents, and the relaxation time of the dynamic compatibility condition on the interface. Relationships among various quasi-static poroelastic parameters are developed. It is shown that local fluid flow mechanism is significant only in the porous media with local heterogeneities. The relaxation time of the compatibility condition on the interface depends upon the details of local structure of porous media that control local fluid pressure diffusion. The new model is used to describe the velocity dispersion and attenuation in fully saturated porous media. The proposed model provides a theoretical framework to simulate the acoustical behavior of fully saturated porous media over a wide range of frequencies without making any explicit assumption about the structure of local heterogeneities.

Keywords: Porous media; Viscoelasticity; Local fluid flow; Constitutive behavior; Velocity dispersion; Attenuation

* Corresponding author. Tel.: +1 405 325 4247; fax: +1 405 325 4217.
E-mail address: muralee@ou.edu (K.K. Muraleetharan).

0020-7683/$ - see front matter © 2005 Elsevier Ltd. All rights reserved.
doi:10.1016/j.ijsolstr.2005.06.008

1. Introduction

Natural porous media such as rocks and sediments in the earth generally have heterogeneity in their material properties at different spatial scales. When a stress wave passes through a heterogeneous porous medium saturated by a fluid, pore fluids existing in different regions respond with different changes in their pore pressures. An internal pore pressure equilibrating process then takes place leading to pore fluid flowing from higher pressure regions to lower pressure regions. According to the distance over which fluid pressure try to equilibrate, three regimes of fluid flow can be identified (Cleary, 1978; Pride et al., 2003). Macroscopic (wavelength-scale) flow is driven by fluid pressure gradient developing at the peak and trough of the stress wave. At microscopic (pore) scales, the fluid is squeezed out of or taken into microcracks and broken grain contacts (Mavko and Nur, 1975; O'Connell and Budiansky, 1977). At meso-scales, which are much larger than pore sizes but much smaller than the wavelength, due to heterogeneities such as variations in lithology and porosity, internal fluid flow occurs from the more compliant high-pressure regions to the relatively stiff low-pressure regions.

It has been recognized that, while Biot's theory of poroelasticity (Biot, 1956a,b, 1962) very well describes the effects of macroscopic flow, it fails to address the effects of local (either microscopic or mesoscopic) fluid flow on the acoustical behavior of porous media with local heterogeneities (Winkler, 1985; Gist, 1994). As a consequence, much research has been devoted to extend or modify some aspects of Biot's theory to account for the effects of local fluid flow. Generally two approaches are taken to account for local fluid flow. The first approach explicitly considers the spatial heterogeneities such as fine layering and inclusions (Gurevich et al., 1997, 1998); the second approach considers viscoelasticity associated with local fluid pressure diffusion in different ways as described below.

Traditionally, the viscoporoelastic behavior related to microscopic flow was investigated by examining the fluid flow in an individual crack (Mavko and Nur, 1975; O'Connell and Budiansky, 1977), or in a grain contact area (Murphy et al., 1986). The effective material properties derived from these procedures depend upon the details of microstructure that are difficult to quantify. More recently, an effective way of analyzing microscopic flow was adopted by Dvorkin and Nur (1993), Dvorkin et al. (1995). In this procedure, microscopic apertures such as microcracks and grain contacts are taken to be crack-like compliant pores, which are assumed to be arranged perpendicular to the direction of compression. Fluid flow inside the crack-like pores is then characterized and incorporated into Biot's theory. Interestingly, Dvorkin et al. (1995) showed that the viscoelasticity induced by microscopic flow can be characterized using a frequency-independent parameter Z, which indeed is the square root of the characteristic time of microscopic flow. This approach does not, however, consider mesoscopic fluid flow.

In an attempt to address mesoscopic fluid flow in fully saturated rocks, Pride and Berryman (2003a,b) and Pride et al. (2004) have developed a double-porosity theory in which the material is viewed as a composite of two isotropic porous solids. One of the essential components of this theory is the dynamic evolution equation controlling the internal fluid transfer between the two porous phases. In this context, the effective properties characterizing the overall viscoelastic behavior of the composite are expressed as functions of the properties of individual constituents and the characteristic size of the embedding solid phase. The complexity of this theory is likely to increase drastically with increasing heterogeneity.

Here, we provide an alternative procedure to characterize the effects of local fluid flow on the acoustical behavior of fully saturated porous media. Our procedure is formulated within the framework of the theory of Biot's poroelasticity (Biot, 1962), but based on volume averaging of microscopic equations. In contrast to previous theories, *the proposed procedure makes no assumption on the local structure of heterogeneities* controlling local fluid flow, and the corresponding material properties can be easily obtained. The essential step in our derivations is to characterize the effect of local fluid flow by the notion of the dynamic compatibility condition on the interface between the solid and the fluid (Wei and Muraleetharan, 2002a). Information on

the details of local heterogeneity is shown to be collectively stored in the relaxation time of the dynamic compatibility condition.

The paper is separated into two parts. The first part deals with constitutive equations and material properties, where the complex, frequency-dependent material properties characterizing the viscoelasticity due to local fluid flow are evaluated. In the second part, the new model is applied to describe the acoustical velocity dispersion and attenuation, from which the information on the local structures of heterogeneities is extracted. In Section 2, a continuum theory of porous media is first introduced, where energy dissipation induced by pore fluid flow is analyzed, and the dynamic compatibility condition on the interface between solid and fluid is introduced. In Section 3, linear constitutive equations are developed within the framework of Biot's theory of poroelasticity; and complex, frequency-dependent material parameters are derived. In Section 4, various relationships among quasi-static poroelastic parameters are developed, and the condition of local homogeneity is discussed. In Section 5, the relaxation time of the dynamic compatibility condition is developed from the micromechanics point of view. In Section 6, the seismic dispersion equation is presented. In Section 7, effects of the relaxation time on the acoustical behavior of porous media are discussed through numerical examples. In Section 8, the new model is applied to describe the measured acoustical velocity dispersion and attenuation of fluid-saturated porous rocks.

2. Theory

The theoretical developments given below follow a macroscopic approach. Hence, unless otherwise specified, all variables are macroscopic quantities. Macroscopic balance equations and state variables are obtained by averaging their microscopic counterparts over an *averaging volume* (see, for example, Hassanizadeh and Gray, 1979a,b). In this paper, a porous medium is viewed as a *macroscopically* isotropic, homogeneous porous continuum, which is a superposition of a solid matrix (S) and a pore fluid (W).

2.1. The effective volume fraction of the pore fluid

Under fully saturated conditions, the volume fraction n^{W} of pore fluid is usually assumed to be equal to the porosity of a porous medium. In a porous medium with local heterogeneities such as different porous phase inclusions, microscopic grain cracks, and broken grain-to-grain contacts (see Fig. 1), however, the meaning of the fluid volume fraction is quite subtle. The behavior of the fluid in the pore space of the local heterogeneities is different from that of the fluid in the surrounding pores, though these two parts of pore fluid can exchange mass. To distinguish these two regions of pore fluid, we generalize the concepts of stiff porosity and soft porosity originally proposed by Dvorkin et al. (1995). Here the soft porosity n_{so} is defined

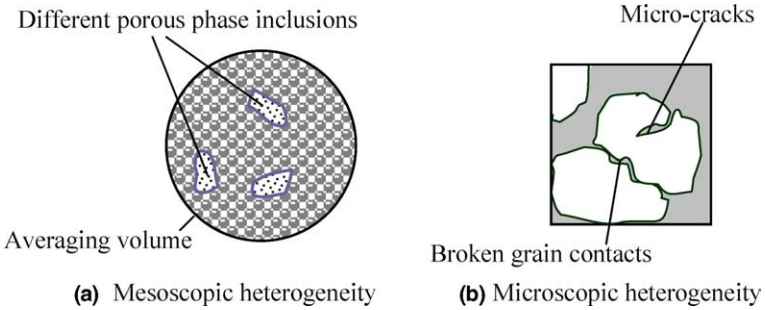

Fig. 1. Local heterogeneities in porous media: (a) mesoscopic heterogeneity; (b) microscopic heterogeneity.

as the ratio of the volume of the pore fluid *trapped* in the local heterogeneities to the total volume of the porous medium, while the stiff porosity n_{st} is the ratio of the volume of the remainder of pore fluid to the total volume of the porous medium. Therefore, the total porosity n is equal to the sum of n_{st} and n_{so}.

In the following, n^W is unambiguously designated as same as the stiff porosity n_{st} and it is called the *effective* volume fraction of the pore fluid. It is assumed that the soft porosity is much smaller than the rigid one so that the latter is very close to the total porosity n (i.e., $n^W = n_{st} \approx n$). This assumption is reasonable for many porous rocks (e.g., Mavko and Jizba, 1991). The small portion of pore fluid trapped in the soft pores is considered as a part of the solid constituent. It is important to note that the use of the effective volume fraction has an important implication in the theory developed here.

To further explore this idea, consider a special case where the solid matrix is rigid, i.e., the total porosity is a constant, and the pore pressure is subjected to an alteration. Due to the fluid pressure imbalance between the local heterogeneities and the surrounding pore space, fluid mass exchange (i.e., local fluid flow) between these two regions will take place. This implies that the effective volume fraction n^W is subjected to change (though very slightly!) and the change of n^W is independent of the skeletal deformation and the compression of solid grains (since n is constant). It is clear that the actual amount of n^W depends on the frequency of the fluid pressure alteration. Under static conditions (i.e., in the low-frequency limit), n^W becomes the maximum, since maximum amount of fluid mass will be exchanged between the two bodies of fluid. In the high-frequency limit, n^W is the minimum, since no mass exchange occurs.

From what is discussed above, in modeling deformable porous media, the effective volume fraction n^W must be generally viewed as an independent state variable that accounts for the mass exchange between the pore space of the local heterogeneities and the surrounding pores. This is one of the distinguished features of the theory developed in this paper.

2.2. State equations

To derive the constitutive equations for a porous media, we shall first establish the state equations of the solid constituent and the pore fluid. These equations have been developed previously by the authors based upon a continuum theory of mixtures with interfaces (Muraleetharan and Wei, 1999; Wei and Muraleetharan, 2002a,b), and will be summarized here.

From the standpoint of the mixture theory of porous media, the total stress tensor $\boldsymbol{\sigma}$ of a porous material can be partitioned into:

$$\boldsymbol{\sigma} = n^S \boldsymbol{\sigma}^S - n^W p^W \boldsymbol{1} \tag{1}$$

where $\boldsymbol{1}$ is the second-order symmetric identity tensor with components represented by Kronecker delta δ_{ij}; n^S is the effective volume fraction of the solid and related to n^W or n through $n^S = 1 - n^W$ ($\approx 1 - n$); $\boldsymbol{\sigma}^S$ is the intrinsic stress tensor of the solid phase; p^W is the pore fluid pressure.

The state equations are given by

$$\boldsymbol{\sigma}^S = \rho^S \frac{\partial A^S}{\partial \boldsymbol{\varepsilon}} - p^S \boldsymbol{1} \tag{2}$$

$$p^S = (\rho^S)^2 \frac{\partial A^S}{\partial \rho^S}, \quad p^W = (\rho^W)^2 \frac{\partial A^W}{\partial \rho^W} \tag{3}$$

where $\boldsymbol{\varepsilon}$ is the infinitesimal strain tensor of the solid matrix; A^S and A^W are the free energy densities (per unit mass) of the solid constituent and the fluid, respectively. Eq. (2) implies that the intrinsic stress tensor $\boldsymbol{\sigma}^S$ of the solid constituent has two contributions: one is related to the skeletal deformation ($\boldsymbol{\varepsilon}$), and the other (denoted as p^S) is associated with the compression of the solid material (the compression of the solid material is represented by its mass density ρ^S). It is noted that the two contributions of $\boldsymbol{\sigma}^S$ are generally coupled. The

standard solid mechanics sign convention, i.e., tensile stresses and strains are positive, is used here and through out the paper.

The free energy densities are assumed to be given by the following functions:

$$A^{\mathrm{S}} = A^{\mathrm{S}}(\boldsymbol{\varepsilon}, \rho^{\mathrm{S}}) \tag{4}$$

$$A^{\mathrm{W}} = A^{\mathrm{W}}(n^{\mathrm{W}}, \rho^{\mathrm{W}}) = U(n^{\mathrm{W}}) + H(\rho^{\mathrm{W}}) \tag{5}$$

where ρ^{W} is the mass density of the fluid. State equations similar to (2) and (3) had been derived by Berryman and Thigpen (1985) based on the variational principle. In this paper, however, in order to account for the local fluid flow as described in Section 2.1, the free energy of pore fluid is assumed to depend explicitly on n^{W} in addition to ρ^{W}.

2.3. Energy dissipation induced by fluid flow

Given state equations (2) and (3) and with assumptions (4) and (5), the rate of energy dissipation due to pressure relaxation and fluid flow can be expressed as (Wei and Muraleetharan, 2002a)

$$\xi = \widehat{\Pi}\dot{n}^{\mathrm{W}} - \widehat{\boldsymbol{\tau}} \cdot (\boldsymbol{v}^{\mathrm{W}} - \boldsymbol{v}^{\mathrm{S}}) \geqslant 0 \tag{6}$$

where $\dot{n}^{\mathrm{W}}$ is the rate of change of the effective volume fraction; $\boldsymbol{v}^{\mathrm{S}}$ and $\boldsymbol{v}^{\mathrm{W}}$ are the velocities of the solid and the fluid, respectively; $\widehat{\boldsymbol{\tau}}$ is the drag force induced by the fluid flow with respect to the solid matrix; $\widehat{\Pi}$ is the unbalanced pressure difference given by

$$\widehat{\Pi} = p^{\mathrm{W}} - p^{\mathrm{S}} - (p^{\mathrm{W}} - p^{\mathrm{S}})_{\mathrm{eq}} \tag{7}$$

Here

$$(p^{\mathrm{W}} - p^{\mathrm{S}})_{\mathrm{eq}} = n^{\mathrm{W}}\rho^{\mathrm{W}}\frac{\partial A^{\mathrm{W}}}{\partial n^{\mathrm{W}}} \tag{8}$$

is the pressure difference at equilibrium. As discussed below, the first term in the right-hand side of Eq. (6) represents the rate of energy dissipation due to local fluid-pressure relaxation (i.e., local fluid flow), while the second term is induced by macroscopic fluid flow.

To understand these two processes of energy dissipation, we shall first analyze the micro-interactions within an averaging volume of the porous medium (Fig. 1a). The size of the averaging volume is assumed to be comparable to the wavelength of concern. At microscopic (pore) scales, when the pore fluid moves with respect to the solid grains, a viscous boundary layer begins to develop in the pores and microscopic viscous forces will be generated, acting on the direction *tangential* to the grain boundaries. In the directions *normal* to the grain boundaries, the pressure compatibility condition requires that the microscopic pressure $p_{\mathrm{m}}^{\mathrm{S}}$ of the solid grain be equal to that of the pore fluid (i.e., $p_{\mathrm{m}}^{\mathrm{W}}$). These two types of microscopic interactions can be linked to two types of macroscopic interactions as discussed below.

Suppose that a stress wave passes through a porous medium. Then a pressure gradient will be generated between the peak and trough of the stress wave, leading to macroscopic (wavelength-scale) fluid flow across the averaging volume. As discussed above, due to the movement of the pore fluid with respect to the solid, a viscous boundary layer begins to develop in the pores if the frequency is larger than a certain value. This kind of viscous drag forces results in wave energy dissipation. The frequency for the onset of the viscous boundary layer is known to be approximately equal to the characteristic frequency ω_{B} at which maximum energy dissipation occurs due to macroscopic fluid flow (Johnson et al., 1987). It is therefore suggested that the microscopic viscous drag forces acting tangentially on the solid grain boundaries are induced by macroscopic fluid flow. At macroscopic level, these drag forces can be collectively represented by $\widehat{\boldsymbol{\tau}}$ in Eq. (6), and can be characterized using Biot's theory (Biot, 1956a,b). The characteristic angular frequency of

macroscopic flow is approximately given by $\omega_B \approx n\eta_W/(\rho^W k)$, where η_W the dynamic viscosity of the fluid, and k the permeability.

Now consider the macroscopic pressures of the solid and the fluid constituents in the averaging volume introduced above. Because of the pressure compatibility, some sort of pressure balance exists between the solid constituent and the fluid. This pressure compatibility can be represented by Eq. (8), which is the macroscopic counterpart of the microscopic pressure compatibility condition on the solid boundaries. When a stress wave passes through the porous medium, due to the fluid mass exchange (i.e., local fluid flow) between the local heterogeneities and the surrounding pores, the pressures of the solid and the fluid will be redistributed over the averaging volume. The pressure redistribution can be considered as a relaxation process that is governed by the local fluid flow, either microscopic or mesoscopic, depending on the frequency of the stress wave. As a consequence, the pressure difference $(p^W - p^S)$ is generally a rate-dependent quantity. Its magnitude depends on the frequency. At the low-frequency limit, local pressure-diffusion processes will be completed within the half the period of the stress wave and no pressure imbalance will be generated in the averaging volume. In general, however, local pressure imbalance will exist in the averaging volume, and local pressure-relaxation processes will take place. These relaxation processes can attenuate wave energy as represented by the first term in the right-side of Eq. (6).

Assume that energy dissipation follows a linear law. As a first approximation and for isotropic porous media, it is assumed based on Eq. (6) that

$$\widehat{\boldsymbol{\tau}} = -\mu(\boldsymbol{v}^W - \boldsymbol{v}^S), \quad \widehat{\Pi} = \zeta \dot{n}^W \tag{9}$$

where μ and ζ are positive material coefficients. For the fluid flow of Poiseiulle type, μ is given by

$$\mu = \frac{(n^W)^2 \eta_W}{k} \tag{10}$$

In practice, however, the assumption of Poiseiulle flow is not always valid. Rather, coefficient μ depends generally upon frequency and the microstructure inside the pores (Biot, 1956b; Johnson et al., 1987). Because our main objective is to address the effects of local fluid flow, it is assumed for convenience that the pore fluid obeys Poiseiulle flow and Eq. (10) applies. Also, it is assumed that ζ is independent of frequency. Now the pressure difference $(p^W - p^S)$ is given by

$$p^W - p^S = (p^W - p^S)_{eq} + \zeta \dot{n}^W \tag{11}$$

Eq. (11) can be considered as the macroscopic counterpart of the *dynamic* compatibility condition on the solid grain boundaries. This equation will play a key role in the following derivations.

3. Linear constitutive equations

3.1. Linearization of the theory

Assume that the porous medium under consideration is initially at an equilibrium state, which is characterized by state parameters: n_0^S, n_0^W, ρ_0^S, ρ_0^W and $\boldsymbol{u}_0^S$. Here $\boldsymbol{u}_0^S$ is the initial displacement of the solid matrix. Under a small disturbance, the state parameters are changed by Δn^W, $\Delta\rho^S$, $\Delta\rho^W$ and $\Delta\boldsymbol{u}^S$, where $\Delta()$ represents the incremental value of a quantity. To derive linear constitutive equations, it is sufficient to assume the following quadratic forms for free energy density functions:

$$n_0^S \rho_0^S \Delta A^S = \frac{1}{2} n_0^S \Delta\boldsymbol{\varepsilon}(\boldsymbol{D} : \Delta\boldsymbol{\varepsilon}) + n_0^S \lambda' \frac{\Delta\rho^S}{\rho_0^S} \Delta\boldsymbol{\varepsilon} : \boldsymbol{I} + \frac{1}{2} n_0^S K_S \left(\frac{\Delta\rho^S}{\rho_0^S}\right)^2 \tag{12}$$

$$n_0^W \rho_0^W \Delta A^W = \frac{1}{2} n_0^W K_W \left(\frac{\Delta\rho^W}{\rho_0^W}\right)^2 + \frac{1}{2} \Theta_W (\Delta n^W)^2 \tag{13}$$

where λ', K_S, K_W and Θ_W are material constants; for isotropic porous media, $\boldsymbol{D}$ is a fourth-order tensor with components given by $\lambda_S\delta_{ij}\delta_{kl} + \mu_S(\delta_{ik}\delta_{jl} + \delta_{il}\delta_{jk})/2$, where λ_S and μ_S are material constants.

The linear counterparts of state equations (2) and (3) can now be written as

$$\Delta\boldsymbol{\sigma}^S = (\lambda_S - \lambda')(\Delta\boldsymbol{\varepsilon} : \boldsymbol{1})\boldsymbol{1} + 2\mu_S\Delta\boldsymbol{\varepsilon} - (K_S - \lambda')\frac{\Delta\rho^S}{\rho_0^S}\boldsymbol{1} \tag{14}$$

$$\Delta p^S = \lambda'\Delta\boldsymbol{\varepsilon} : \boldsymbol{1} + K_S\frac{\Delta\rho^S}{\rho_0^S} \tag{15}$$

$$\Delta p^W = K_W\frac{\Delta\rho^W}{\rho_0^W} \tag{16}$$

and Eq. (8) becomes

$$(\Delta p^W - \Delta p^S)_{eq} = \Theta_W\Delta n^W \tag{17}$$

Clearly, parameters K_S and K_W are the *effective* bulk moduli of the solid material and the fluid, respectively. Constant λ' characterizes the coupling effects between the compression of solid material and the deformation of solid matrix. Constant Θ_W is the change in pressure difference $(p^W - p^S)$ solely due to a unit change in n^W under static conditions. For later reference, the linear mass balance equation of c-phase (c = S, W) is introduced as

$$n_0^c\frac{\Delta\rho^c}{\rho_0^c} + \Delta n^c + n_0^c\nabla\cdot(\Delta\boldsymbol{u}^c) = 0 \tag{18}$$

3.2. Quasi-static response

Under quasi-static (low-frequency) conditions, no local unbalanced pressure is generated in the porous medium as discussed above. In this case, $\widehat{\Pi} = 0$, and the time-dependent behavior of porous media is solely due to macroscopic fluid diffusion. Displacement fields $\boldsymbol{u}^S$ and $\boldsymbol{u}^W$ are chosen as independent state variables. By eliminating $\Delta\rho^c$ and Δn^c (c = S, W) from (14)–(18), it follows after some manipulations that

$$n_0^S\Delta\boldsymbol{\sigma}^S = [A\Delta\boldsymbol{\varepsilon} : \boldsymbol{1} + Q\nabla\cdot(\Delta\boldsymbol{u}^W)]\boldsymbol{1} + 2G\Delta\boldsymbol{\varepsilon} \tag{19}$$

$$n_0^W\Delta p^W = -Q\Delta\boldsymbol{\varepsilon} : \boldsymbol{1} - R\nabla\cdot(\Delta\boldsymbol{u}^W) \tag{20}$$

where $G(= n_0^S\mu_S)$ is the shear modulus of the porous matrix; coefficients A, Q, and R are related to K_S, K_W, λ_S, μ_S, λ', and Θ_W as below:

$$A = \widehat{K} - \frac{2}{3}G + \frac{(n_0^S)^2(K_S - \lambda')^2(K_W + n_0^W\Theta_W)}{K_S[n_0^WK_S + n_0^S(K_W + n_0^W\Theta_W)]} \tag{21}$$

$$Q = \frac{n_0^Sn_0^WK_W(K_S - \lambda')}{n_0^WK_S + n_0^S(K_W + n_0^W\Theta_W)} \tag{22}$$

$$R = \frac{(n_0^W)^2K_W(K_S + n_0^S\Theta_W)}{n_0^WK_S + n_0^S(K_W + n_0^W\Theta_W)} \tag{23}$$

and

$$\widehat{K} = n_0^S\left(\lambda_S + \frac{2}{3}\mu_S\right) - \frac{n_0^S(\lambda')^2}{K_S} \tag{24}$$

For the purpose of comparison, the notations of Biot (1956a) are used here for the elastic parameters. One can observe from Eqs. (19) and (20) that for fully saturated isotropic porous media, there are four independent material parameters, i.e., A, Q, R, and G, which have to be determined.

The fluid mass content m^{W} can also be introduced as a state variable. Note that

$$\frac{\Delta m^{\mathrm{W}}}{\rho_0^{\mathrm{W}}} = -\nabla \cdot [n_0^{\mathrm{W}}(\Delta \boldsymbol{u}^{\mathrm{W}} - \Delta \boldsymbol{u}^{\mathrm{S}})] \tag{25}$$

where $\Delta m^{\mathrm{W}}/\rho_0^{\mathrm{W}}$ represents the volume of the fluid entering the pores in a unit volume of bulk material. With Eqs. (1), (19) and (20), one can derive:

$$\Delta \boldsymbol{\sigma} = \left[\left(K_{\mathrm{U}} - \frac{2}{3}G\right)\Delta \boldsymbol{\varepsilon} : \boldsymbol{I} - \alpha_{\mathrm{B}}\mathsf{M}\frac{\Delta m^{\mathrm{W}}}{\rho_0^{\mathrm{W}}}\right]\boldsymbol{I} + 2G\Delta \boldsymbol{\varepsilon} \tag{26}$$

$$\Delta p^{\mathrm{W}} = \mathsf{M}\left(-\alpha_{\mathrm{B}}\Delta \boldsymbol{\varepsilon} : \boldsymbol{I} + \frac{\Delta m^{\mathrm{W}}}{\rho_0^{\mathrm{W}}}\right) \tag{27}$$

where K_{U} is the *undrained* bulk modulus of the porous material, M the fluid storage coefficient, and α_{B} the effective stress coefficient. Parameters M and α_{B} are given by

$$\frac{1}{\mathsf{M}} = \frac{n_0^{\mathrm{S}}}{K_{\mathrm{S}} + n_0^{\mathrm{S}}\Theta_{\mathrm{W}}} + \frac{n_0^{\mathrm{W}}}{K_{\mathrm{W}}} \tag{28}$$

$$\alpha_{\mathrm{B}} = 1 - \frac{n_0^{\mathrm{S}}(\lambda' + n_0^{\mathrm{S}}\Theta_{\mathrm{W}})}{(K_{\mathrm{S}} + n_0^{\mathrm{S}}\Theta_{\mathrm{W}})} \tag{29}$$

Eliminating $\Delta m^{\mathrm{W}}/\rho_0^{\mathrm{W}}$ from Eqs. (26) and (27) yields

$$\Delta \boldsymbol{\sigma} + \alpha_{\mathrm{B}}\Delta p^{\mathrm{W}}\boldsymbol{I} = \left(K_{\mathrm{D}} - \frac{2}{3}G\right)(\Delta \boldsymbol{\varepsilon} : \boldsymbol{I})\boldsymbol{I} + 2G\Delta \boldsymbol{\varepsilon} \tag{30}$$

where K_{D} is the *drained* bulk modulus and given by

$$K_{\mathrm{D}} = K_{\mathrm{U}} - \mathsf{M}\alpha_{\mathrm{B}}^2 = \widehat{K} + n_0^{\mathrm{S}}(K_{\mathrm{S}} - \lambda')^2\left[\frac{1}{K_{\mathrm{S}}} - \frac{1}{K_{\mathrm{S}} + n_0^{\mathrm{S}}\Theta_{\mathrm{W}}}\right] \tag{31}$$

Clearly, K_{D} equals $\widehat{K}$ when Θ_{W} vanishes. As shown in Section 4.2, this is the case when porous media are locally homogeneous.

In the constitutive relationships presented above, there are six elastic parameters, i.e., K_{S}, K_{W}, λ_{S}, μ_{S}, λ' and Θ_{W}. Although the static behavior of saturated porous materials can be fully characterized by using only four independent poroelastic parameters, e.g., G, K_{U}, M and α_{B}, we shall show later that these six parameters play a key role in evaluating the dynamic properties of porous media.

3.3. Dynamic response

In general, free fluid filtration is locally prohibited in the pore space of local heterogeneities such as micro-cracks and broken grain contacts. When the characteristic time of local fluid-pressure relaxation is comparable to or larger than the characteristic time of loading the effect of the local pressure relaxation in local heterogeneities becomes significant. As a consequence, the porous medium as whole behaves as a viscoelastic solid, and its macroscopic behavior is frequency-dependent.

By virtue of Eq. (17), the linear form of Eq. (11) can be written as

$$\Delta p^{\mathrm{W}} - \Delta p^{\mathrm{S}} = \Theta_{\mathrm{W}}(\Delta n^{\mathrm{W}} + \tau_{\mathrm{W}}\Delta \dot{n}^{\mathrm{W}}) \tag{32}$$

where τ_W ($=\zeta/\Theta_W$) is the relaxation time of local fluid pressure. To derive the complex, frequency-dependent parameters that characterize viscoporoelasticity, one assumes that all state variables have $e^{-i\omega t}$ time dependence. Eq. (32) now becomes

$$\Delta p^W - \Delta p^S = \Theta_W(1 - i\omega\tau_W)\Delta n^W \tag{33}$$

where ω is the angular frequency and $i^2 = -1$. This equations implies that pressure difference change ($\Delta p^W - \Delta p^S$) is frequency-dependent as discussed in Section 2.3.

Based on the principle of correspondence (Biot, 1962), one can derive the linear constitutive equations similar to those given in Section 3.2 (i.e., Eqs.(19), (20), (26), (27) and (30)). Now the material parameters in the constitutive equations are complex and frequency-dependent. The only difference between the quasi-static and dynamic model presented above exists in Eq. (33). By comparing (33) to (17), it is clear that the complex material parameters can be obtained by replacing Θ_W for $\Theta_W(1 - i\omega\tau_W)$ in their quasi-static counterparts. For instance, corresponding to (28), (29) and (31), one can write:

$$\frac{1}{\widetilde{M}(\omega)} = \frac{n_0^S}{K_S + n_0^S\Theta_W(1 - i\omega\tau_W)} + \frac{n_0^W}{K_W} \tag{34}$$

$$\tilde{\alpha}_B(\omega) = 1 - \frac{n_0^S[\lambda' + n_0^S\Theta_W(1 - i\omega\tau_W)]}{[K_S + n_0^S\Theta_W(1 - i\omega\tau_W)]} \tag{35}$$

$$\widetilde{K}_U(\omega) = \widetilde{M}\tilde{\alpha}_B^2 + \widehat{K} + \left[\frac{n_0^S(K_S - \lambda')^2}{K_S} - \frac{n_0^S(K_S - \lambda')^2}{K_S + n_0^S\Theta_W(1 - i\omega\tau_W)}\right] \tag{36}$$

where quantities with a caret "$\sim$" are complex numbers.

Compared to the quasi-static poroelastic model discussed in Section 3.2, viscoporoelastic model depends upon an additional material parameter, i.e., the relaxation time τ_W. As discussed in Section 5, the parameter τ_W is a function of the local structure of porous media that controls local fluid flow. In the model presented here the frequency-dependent behavior of a porous material is taken into account only through Eq. (33). Constants K_S, K_W, λ_S, μ_S, λ', Θ_W and τ_W are assumed to be independent of frequency.

4. Quasi-static poroelastic parameters

To determine the complex, frequency-dependent material properties, one must first evaluate parameters K_S, K_W, λ_S, μ_S, λ', Θ_W and τ_W. Suppose that the effective bulk moduli of the solid material and the fluid, i.e., K_S and K_W, are known, and μ_S is obtained by measuring the shear modulus G of the porous medium. Next we will evaluate λ_S, λ' and Θ_W. Because these elastic constants are independent of frequency, they can be determined under quasi-static conditions ($\omega \approx 0$). To this end, compression tests can be conducted to measure three quasi-static poroelastic parameters such as the drained and undrained bulk moduli of the porous medium. These tests include undrained compression, drained compression, and unjacketed compression tests (Kümpel, 1991).

4.1. Porous media with local heterogeneities

First consider a porous medium with local heterogeneities. Through compression tests, one can measure poroelastic parameters including undrained bulk modulus K_U, drain bulk modulus K_D, pore pressure coefficient B and effective stress coefficient α_B, as well as the pore compressibility C_n and the unjacketed compressibility C_S^* (or unjacketed bulk modulus K_S^* of the solid matrix). The latter two are defined by

$$C_n = -\frac{1}{V_n}\left(\frac{\partial V_n}{\partial p^{\mathrm{W}}}\right)_{p_{\mathrm{c}}=p^{\mathrm{W}}}, \quad C_{\mathrm{S}}^{*} = \frac{1}{K_{\mathrm{S}}^{*}} = -\frac{1}{V}\left(\frac{\partial V}{\partial p^{\mathrm{W}}}\right)_{p_{\mathrm{c}}=p^{\mathrm{W}}} \tag{37}$$

where V and V_n are the total and pore volumes, respectively, in an averaging volume of the porous medium; p_{c} is the confining (or total) pressure. Lade and de Boer (1997) introduced two other compressibility parameters, defined by

$$C_{\mathrm{S}}^{\mathrm{u}} = -\frac{1}{V_{\mathrm{S}}}\left(\frac{\partial V_{\mathrm{S}}}{\partial p^{\mathrm{W}}}\right)_{p_{\mathrm{d}}}, \quad C_{\mathrm{S}}^{\mathrm{d}} = -\frac{1}{V_{\mathrm{S}}}\left(\frac{\partial V_{\mathrm{S}}}{\partial p_{\mathrm{d}}}\right)_{p^{\mathrm{W}}} \tag{38}$$

where V_{S} is the volume of the solid material. Here, p_{d} $(=p_{\mathrm{c}} - p^{\mathrm{W}})$ is the intergranular pressure. Parameters $C_{\mathrm{S}}^{\mathrm{u}}$ and $C_{\mathrm{S}}^{\mathrm{d}}$ represent the compressibility of the solid material due to changes in p^{W} and p_{d}, respectively.

Next, we shall show that generally there are three independent parameters among those measured through the above-mentioned compression tests, provided that the fluid bulk modulus K_{W} is known. From the definitions of C_n, C_{S}^{*} and $C_{\mathrm{S}}^{\mathrm{u}}$, it immediately follows that

$$C_{\mathrm{S}}^{\mathrm{u}} = \frac{1}{n_0^{\mathrm{S}}}(C_{\mathrm{S}}^{*} - n_0^{\mathrm{W}} C_n) \tag{39}$$

Also, one can write

$$C_{\mathrm{S}}^{\mathrm{d}} = C_{\mathrm{S}}^{*} \tag{40}$$

To derive expression (40), one can first use (14)–(17) to obtain

$$\Delta p_{\mathrm{d}} = -n_0^{\mathrm{S}}\left(\lambda_{\mathrm{S}} + \frac{2}{3}\mu_{\mathrm{S}} + n_0^{\mathrm{S}}\Theta_{\mathrm{W}}\right)\Delta\boldsymbol{\varepsilon} : \boldsymbol{I} - n_0^{\mathrm{S}}(\lambda' + n_0^{\mathrm{S}}\Theta_{\mathrm{W}})\frac{\Delta\rho^{\mathrm{S}}}{\rho_0^{\mathrm{S}}} \tag{41}$$

$$\Delta p^{\mathrm{W}} = (\lambda' + n_0^{\mathrm{S}}\Theta_{\mathrm{W}})\Delta\boldsymbol{\varepsilon} : \boldsymbol{I} + (K_{\mathrm{S}} + n_0^{\mathrm{S}}\Theta_{\mathrm{W}})\frac{\Delta\rho^{\mathrm{S}}}{\rho_0^{\mathrm{S}}} \tag{42}$$

Using the definitions and noting that $\Delta V/V = \Delta\boldsymbol{\varepsilon}:\boldsymbol{I}$, $\Delta V_{\mathrm{S}}/V_{\mathrm{S}} = -\Delta\rho^{\mathrm{S}}/\rho_0^{\mathrm{S}}$, and $V_{\mathrm{S}}/V = n_0^{\mathrm{S}}$, one derives:

$$C_{\mathrm{D}} = \frac{(K_{\mathrm{S}} + n_0^{\mathrm{S}}\Theta_{\mathrm{W}})}{\Psi} \tag{43}$$

$$C_{\mathrm{S}}^{\mathrm{d}} = C_{\mathrm{S}}^{*} = \frac{n_0^{\mathrm{S}}(\lambda' + n_0^{\mathrm{S}}\Theta_{\mathrm{W}})}{\Psi} \tag{44}$$

$$C_{\mathrm{S}}^{\mathrm{u}} = \frac{n_0^{\mathrm{S}}(\lambda_{\mathrm{S}} + 2\mu_{\mathrm{S}}/3 + n_0^{\mathrm{S}}\Theta_{\mathrm{W}})}{\Psi} \tag{45}$$

where C_{D} $(=1/K_{\mathrm{D}})$ is the drained compressibility of the solid matrix, and

$$\Psi = n_0^{\mathrm{S}}[(\lambda_{\mathrm{S}} + 2\mu_{\mathrm{S}}/3 + n_0^{\mathrm{S}}\Theta_{\mathrm{W}})(K_{\mathrm{S}} + n_0^{\mathrm{S}}\Theta_{\mathrm{W}}) - (\lambda' + n_0^{\mathrm{S}}\Theta_{\mathrm{W}})^2] \tag{46}$$

Lade and de Boer (1997) measured compressibility parameters C_{D}, C_{S}^{*}, $C_{\mathrm{S}}^{\mathrm{u}}$ and $C_{\mathrm{S}}^{\mathrm{d}}$ for an artificial porous material (i.e., Basswood cubes) subjected to various confining pressures. Lade and de Boer's (1997) results are reproduced in Fig. 2. It can be seen that all the values of C_{S}^{*} are very close to those of $C_{\mathrm{S}}^{\mathrm{d}}$ for all the confining pressures.

By using (43) and (44), the effective stress coefficient (29) becomes:

$$\alpha_{\mathrm{B}} = 1 - \frac{C_{\mathrm{S}}^{*}}{C_{\mathrm{D}}} \tag{47}$$

It is important to note that thus far no restriction has been made on the local structure in porous media. Hence, Eq. (47) is generally valid for isotropic porous media. Nur and Byerlee (1971) obtained

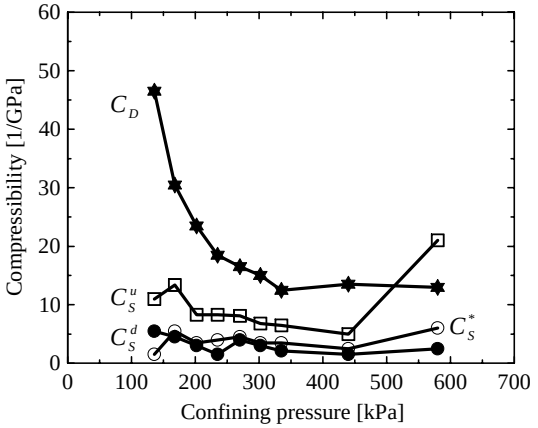

Fig. 2. Compressibility parameters for Basswood cubes subjected to various confining pressures (after Lade and de Boer, 1997).

an expression similar to (47). In their formulation, however, it was assumed that the porous medium of concern is locally homogeneous.

Using (26) and (27), in undrained conditions (i.e., $\Delta m^{\mathrm{W}} = 0$), one obtains:

$$\Delta p^{\mathrm{W}} = -\frac{\mathsf{M}\alpha_{\mathrm{B}}}{K_{\mathrm{U}}}\left(\frac{\Delta\boldsymbol{\sigma} : \boldsymbol{I}}{3}\right) \tag{48}$$

With its very definition, the pore pressure coefficient B is given by

$$B = \frac{\mathsf{M}\alpha_{\mathrm{B}}}{K_{\mathrm{U}}} = \frac{\mathsf{M}\alpha_{\mathrm{B}}}{K_{\mathrm{D}} + \mathsf{M}\alpha_{\mathrm{B}}^2} \tag{49}$$

This is a well-known result in poromechanics (e.g., Coussy, 1995, p. 102). Using (28), (29), (31), (43)–(45) and (49), one can further derive:

$$B = \frac{1}{1 + \frac{n_0^{\mathrm{W}} C_{\mathrm{W}} + n_0^{\mathrm{S}} C_{\mathrm{S}}^{\mathrm{u}} - C_{\mathrm{S}}^*}{C_{\mathrm{D}} - C_{\mathrm{S}}^*}} = \frac{1}{1 + \frac{n_0^{\mathrm{W}}(C_{\mathrm{W}} - C_n)}{C_{\mathrm{D}} - C_{\mathrm{S}}^*}} \tag{50}$$

where C_{W} $(=1/K_{\mathrm{W}})$ is the fluid compressibility. An alternative way to derive Eq. (50) can be found in Berryman (2002).

It can be deduced from Eqs. (39) and (43)–(45) that

$$\Psi = \frac{n_0^{\mathrm{S}}}{C_{\mathrm{D}}(\alpha_{\mathrm{B}} C_{\mathrm{S}}^* - n_0^{\mathrm{W}} C_n)} \tag{51}$$

Now it follows from Eq. (43) that

$$K_{\mathrm{S}} + n_0^{\mathrm{S}}\Theta_{\mathrm{W}} = \frac{n_0^{\mathrm{S}}}{\alpha_{\mathrm{B}} C_{\mathrm{S}}^* - n_0^{\mathrm{W}} C_n} \tag{52}$$

Using Eq. (52), one may cast Eq. (28) into:

$$\frac{1}{\mathsf{M}} = n_0^{\mathrm{W}} C_{\mathrm{W}} + \alpha_{\mathrm{B}} C_{\mathrm{S}}^* - n_0^{\mathrm{W}} C_n \tag{53}$$

This is the most general expression for the fluid storage coefficient M, and hence it is valid for any fully saturated isotropic porous media.

It is now clear that because of (39), (40), (47), (49), (50) and (53), if C_W is determined, there are only three independent parameters among K_U, B, K_D, α_B, C_n, C_S^*, M, C_S^u and C_S^d. With any three of these parameters and if K_S, K_W and G are given, constants λ_S, λ' andΘ_W can be finally determined.

Noting that $K_U = K_D + M\alpha_B^2$ and using Eqs. (47) and (53), one obtains:

$$\frac{1}{C_U - C_S^*} = \frac{1}{C_D - C_S^*} + \frac{1}{n_0^W (C_W - C_n)} \tag{54}$$

where C_U ($=1/K_U$) is the undrained compressibility of the solid matrix. This relationship was first derived by Brown and Korringa (1975), who made use of the reciprocity theorem of elasticity.

4.2. Locally homogeneous porous media

It is now instructive to discuss a special model first introduced by Gassmann (1951), in which the porous medium is assumed to be composed of a solid matrix that is locally homogeneous. In such materials, the strain components along any continuous path across the solid matrix are equal to those within the solid material of the matrix. This assumption was extensively applied in poromechanics (Biot and Willis, 1957; Nur and Byerlee, 1971; Rice and Cleary, 1976).

Consider an averaging volume of a locally homogeneous porous medium that is fully saturated with a liquid. Suppose that the material is *unjacketed* and subjected to a hydrostatic pressure increase Δp_c. The porous material deforms in exact proportion everywhere in the averaging volume. One therefore expects that the porosity will be constant, i.e. $\Delta n = \Delta n^W = 0$. From Eq. (17), it follows that $\Delta p^S = \Delta p^W = \Delta p_c$. Also, in the porous medium, there exist no local heterogeneities such as different soft porous inclusions, broken grain contacts and microcracks; all the pores are interconnected and allow free fluid filtration. In this case, the free energy of the fluid is independent of the porosity. By its very definition, Θ_W vanishes.

Due to local homogeneity, $\Delta\rho^S/\rho_0^S = -\Delta\boldsymbol{\varepsilon} : \boldsymbol{I}$ and $\Theta_W = 0$. In an unjacketed compression test, $\Delta p_d = \Delta p_c - \Delta p^W = 0$. Now it follows from Eq. (41) that

$$\lambda' = \lambda_S + \frac{2}{3}\mu_S \tag{55}$$

Using Eqs. (39), (44) and (45), one can obtain:

$$C_n = C_S^u = C_S^d = C_S^* \tag{56}$$

Since $\Theta_W = 0$, Eq. (50) yields

$$C_S^* = \frac{1}{K_S^*} = \frac{n_0^S}{(\alpha_B - n_0^W)} \frac{1}{K_S} \tag{57}$$

Noting that $n_0^W < \alpha_B \leqslant 1$, it is clear that $C_S^* \geqslant C_S (= 1/K_S)$. Hence, K_S^* is generally less than the effective bulk modulus K_S of the solid material in a porous medium. This discrepancy is apparently due to the coupling between the compressions of the solid material and the matrix.

Applying Eq. (56) to Eq. (53), it immediately follows that

$$\frac{1}{M} = \frac{n_0^W}{K_W} + \frac{\alpha_B - n_0^W}{K_S^*} \tag{58}$$

The well-known Gassmann (1951) equation follows simply by inserting (56) into (54):

$$\frac{1}{C_U - C_S^*} = \frac{1}{C_D - C_S^*} + \frac{1}{n_0^W (C_W - C_S^*)} \tag{59}$$

Expressions (58) and (59) are valid *only* for the porous media that are locally homogeneous. In many applications, however, porous media are heterogeneous, in which small portion of the fluid is trapped in the soft pores such as grain microcracks and broken grain contacts so that free fluid filtration is prohibited in these regions. In such cases, the *effective* volume fraction n^{W} of the fluid may vary in a way discussed in Section 2.1, and the free energy of the pore fluid depends upon n^{W}. By its definition, parameter Θ_{W} now becomes a positive quantity. Therefore, constant Θ_{W} is the parameter that can be used to characterize the local heterogeneity of fully saturated porous materials.

Eq. (56) is an additional constraint imposed by assuming local homogeneity, such that only two parameters are independent among K_{U}, B, K_{D}, α_{B}, C_{n}, C_{S}^{*}, M, C_{S}^{u} and C_{S}^{d}. This fact was first recognized a long time back by Biot and Willis (1957), who pointed out that for homogeneous porous media, there are only three independent poroelastic parameters including G, provided that C_{W} is known. In addition, for the porous media that are locally homogeneous, since Θ_{W} is zero, the effects of local fluid on the poroviscoelastic behavior are negligible. In this case, complex material properties presented in Section 3.3 are real numbers and independent of frequency. This result can be used to explain the experimental observations that Biot's theory predicts very well the seismic response of synthetic porous media made from sintered glass beads, whereas it fails to describe the seismic behavior of natural rocks (Winkler, 1985; Gist, 1994). The reason is that the synthetic porous media are locally homogeneous, whereas the natural rocks generally have local structure.

Because $\lambda_{S} > 0$ and $\Theta_{W} \geqslant 0$, using Eqs. (28), (29) and (31), one obtains the following estimates for K_{S}:

$$\left[n_{0}^{S} - \frac{(1-\alpha_{B})^{2}}{n_{0}^{S}}\right]\left(\frac{1}{M} - \frac{n_{0}^{W}}{K_{W}}\right)^{-1} - \frac{1}{n_{0}^{S}}\left(K_{D} - \frac{2}{3}G\right) < K_{S} \leqslant n_{0}^{S}\left(\frac{1}{M} - \frac{n_{0}}{K_{W}}\right)^{-1} \tag{60}$$

5. Relaxation time of local fluid flow

Thus far, relaxation time τ_{W} has not been evaluated. As described in Section 8, using a trial-and-error procedure, one can determine τ_{W} by comparing the model predictions with the measured seismic data of porous media. This method avoids characterizing the details of local structure of porous materials. In practice, however, it is extremely useful to obtain the information on the local structure of porous media. Let ω_{c} be the characteristic angular frequency of local (microscopic or mesoscopic) fluid flow. Because the pressure relaxation process is governed by local fluid flow, the relaxation time can be approximately written as $\tau_{W} \approx 2\pi/\omega_{c}$.

For microscopic flow in microscopic apertures, such as microcracks and broken grain contacts, there are several formulations of ω_{c} available in the literature (O'Connell and Budiansky, 1977; Cleary, 1978; Mavko and Nur, 1979). These formulations relate the characteristic frequency to a specific type of apertures associated with the microscopic flow. In the following, microscopic apertures are treated as flat cylindrical cavities in the solid phase. This kind of apertures can be used to simulate the broken grain contacts. Following arguments of Johnston et al. (1979), one can obtain the relaxation time of the microscopic flow in flat cylindrical cavities as (see Appendix A):

$$\tau_{W} = \frac{3\eta_{W}}{2K_{W}\alpha^{2}} \tag{61}$$

where α is the typical aspect ratio of the apertures and η_{W} the viscosity of the fluid.

If the aspect ratio α is small, the fluid may be absorbed onto the surface of the solid materials and there will be no free fluid that can flow in response to a seismic wave and produce attenuation. As pointed out by Jones (1986), for natural rocks, if $\alpha < 10^{-4}$, fluid flow in the apertures make no contribution to energy dis-

sipation. With this value of α and for water ($K_W = 2.25$ GPa, $\eta_W = 1$ mPa s), it can be shown that τ_W must be less than 10^{-4} s for the microscopic (squirt) flow dissipation to be active.

For mesoscopic flow, the relaxation time is given by $\tau_W \approx \ell_m^2/D_m$, where ℓ_m is the characteristic size of mesoscopic heterogeneity and D_m is the meso-scale fluid-pressure diffusivity. To be meaningful, ℓ_m should be much less than the wavelength and much larger than the pore size. Keeping in mind that mesoscopic flow is driven by the local gradient of fluid pressure, a simple dimensional analysis yields

$$D_m = \frac{M k_m}{\eta_W} \approx \frac{K_W k}{n_0^W \eta_W} \tag{62}$$

where k_m is the meso-scale permeability and, as a first approximation, it is assumed to equal the global permeability k. It follows that

$$\tau_W \approx \frac{n_0^W \eta_W \ell_m^2}{K_W k} \tag{63}$$

Interestingly, for local fluid flow (either microscopic or mesoscopic), τ_W is proportional to η_W. That is, characteristic frequency f_m ($=1/\tau_W$) of local fluid flow is proportional to ($1/\eta_W$), which is in a sharp contrast to the macroscopic flow. This result is, however, consistent with experimental observations (Winkler, 1985).

6. Dispersion equation of compressional waves

To apply the theory to analyze the acoustical behavior of porous media, we now develop the dispersion equation of compressional waves. Because local flow mechanisms is of primary interest in this paper, the frequency dependence of permeability coefficient and the inertial coupling effects in the sense of Biot (1956a,b) will be neglected.

First the governing equations are presented in the following linear form:

$$\nabla \cdot \boldsymbol{\sigma} = \rho_0 \frac{\partial^2}{\partial t^2} \boldsymbol{u}^S + \rho_0^W \frac{\partial^2}{\partial t^2} \boldsymbol{w} \tag{64}$$

$$-\nabla p^W = \rho_0^W \frac{\partial^2}{\partial t^2} \boldsymbol{u}^S + \left(\frac{\rho_0^W}{n_0^W} \frac{\partial}{\partial t} + \frac{\eta_W}{k} \right) \frac{\partial}{\partial t} \boldsymbol{w} \tag{65}$$

where $\boldsymbol{w}$ ($= n_0^W(\boldsymbol{u}^W - \boldsymbol{u}^S)$) is the filtration displacement such that the time rate of $\boldsymbol{w}$ represents the filtration velocity of the fluid; η_W the dynamic viscosity of the fluid; k the permeability; and ρ_0 is the total initial mass density of the porous media and given by $\rho_0 = n_0^W \rho_0^W + n_0^S \rho_0^S$.

The linear constitutive equations are given by

$$\boldsymbol{\sigma} = \left[(\widetilde{K}_U - \frac{2}{3}\widetilde{G}) \nabla \cdot \boldsymbol{u}^S + \tilde{\alpha}_B \widetilde{M} \nabla \cdot \boldsymbol{w} \right] \boldsymbol{1} + G[\nabla \boldsymbol{u}^S + (\nabla \boldsymbol{u}^S)^T] \tag{66}$$

$$-p^W = \widetilde{M}(\tilde{\alpha}_B \nabla \cdot \boldsymbol{u}^S + \nabla \cdot \boldsymbol{w}) \tag{67}$$

where complex parameters $\widetilde{K}_U$, $\tilde{\alpha}_B$ and $\widetilde{M}$ are given by (34)–(36).

Inserting (66) into (64) and (67) into (65), and following a fairly standard procedure (Biot, 1956a), we obtain the following dispersion equation of compressional waves:

$$\begin{vmatrix} \left(\widetilde{K}_U + \frac{4}{3}G\right)\zeta^2 - \rho\omega^2 & \widetilde{M}\tilde{\alpha}_B\zeta^2 - \rho^W\omega^2 \\ \widetilde{M}\tilde{\alpha}_B\zeta^2 - \rho^W\omega^2 & \widetilde{M}\zeta^2 - \frac{\rho^W}{n_0^W}\omega^2 + \frac{\eta_W}{k}\mathrm{i}\omega \end{vmatrix} = 0 \tag{68}$$

where ζ is the complex wave number with a real part ζ_R and an imaginary part ζ_I. The phase velocity v and attenuation (i.e. the inverse quality factor) Q^{-1} of the compressional waves are defined, respectively, by:

$$v = \frac{\omega}{\zeta_R} \tag{69}$$

$$Q^{-1} = \frac{2\zeta_I}{\zeta_R} \tag{70}$$

Clearly, given a certain frequency, dispersion equation (68) has two meaningful solutions that correspond, respectively, to the first (fast) and the second (slow) compressional waves.

7. Effects of the relaxation time

We now present numerical examples to illustrate the effects of relaxation time τ_W on the compressional waves propagating through fully saturated porous rocks. The material of concern is the D'Euville limestone with a porosity of 0.18. The material properties of D'Euville limestone are summarized in Table 1.

The effects of relaxation time τ_W on the frequency dependence of phase velocity and attenuation of the first compressional (P1) wave are depicted in Fig. 3. For these calculations the properties of D'Euville limestone corresponding to a confining pressure of 5 MPa were used (Table 1). The results for Biot's model are obtained by setting $\tau_W = 0$ s. In contrast to Biot's model, the new model predicts significant velocity dispersion and attenuation due to local fluid flow ($\tau_W \neq 0$). For each τ_W, two peaks can be seen in the frequency dependence of attenuation: the first one is associated with the local fluid flow, and the second one is related to the macroscopic flow (i.e., the Biot flow). An increase in τ_W shifts the attenuation peak associated with the local fluid flow (the peak on the left-hand side) to a lower frequency.

It is clear that the new model describes the energy dissipation due to both local fluid flow and macroscopic fluid flow over a broad range of frequencies. In this example, when τ_W is larger than 0.0001 s, mesoscopic flow is the dominant loss mechanism. Indeed, if $\tau_W > 0.0001$ s, a simple calculation using Eq. (61) yields the typical aspect ratio of apertures as $\alpha < 8 \times 10^{-5}$, at which the effects of microscopic (squirt) flow become trivial (Jones, 1986). If $\tau_W > 0.0001$ s, Eq. (63) yields $\ell_m > 1$ cm. On the other hand, if $\tau_W < 10^{-6}$ s, it follows from (63) that $\ell_m < 1$ mm, which is comparable to the pore size. Hence, for $\tau_W < 10^{-6}$ s microscopic (squirt) flow will be dominant and for 10^{-6} s $< \tau_W < 10^{-4}$ s both micro-scale and meso-scale flows are active.

It can be seen from Fig. 4 that the local fluid flow has very slight influence on the velocity dispersion and attenuation of the second compressional (P2) wave. This result is reasonable, since the slow wave is primar-

Table 1
Material properties of D'Euville limestone (after Lucet, 1989)

Parameter	Symbol	Confining pressure	
		3 MPa	5 MPa
Bulk modulus of solid, GPa	K_S	62.0	62.0
Bulk modulus of water, GPa	K_W	2.25	2.25
Density of solid, kg/m^3	ρ_0^S	2710	2710
Density of water, kg/m^3	ρ_0^W	1000	1000
Permeability, m^2	k	1.0×10^{-13}	1.0×10^{-13}
Viscosity of water, Pa.s	η_W	1.0×10^{-3}	1.0×10^{-3}
Bulk modulus of matrix, GPa	K_D	11.5	16.7
Shear modulus of matrix, GPa	G	9.42	10.2
Effective stress coefficient[a]	α_B	0.75	0.70
Pore pressure coefficient[a]	B	0.46	0.34

[a] α_B and B are estimated based on the equations provided in Section 4.

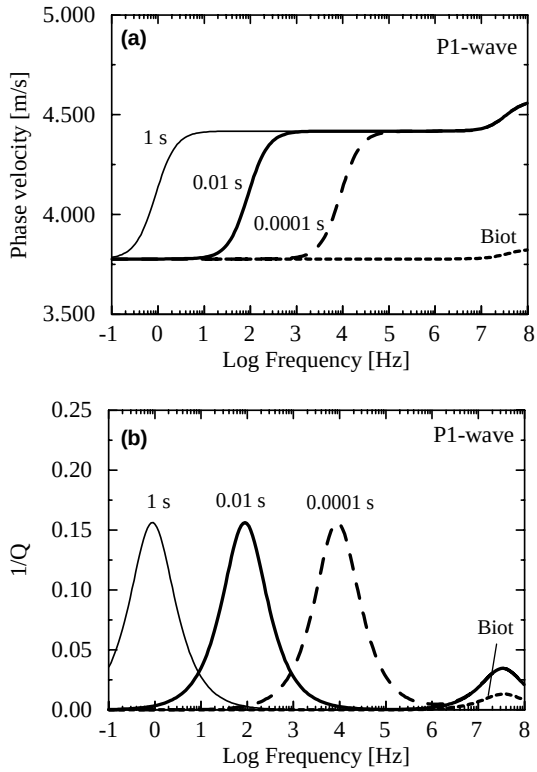

Fig. 3. Influence of the relaxation time (τ_W) on the velocity and attenuation of the P1-wave in a fully saturated D'Euville limestone.

ily associated with the macroscopic motion of the saturating fluid. Hence, the geometry and tortuosity of the pores become the factors influencing the P2-wave (Klimentos and McCann, 1988; Gist, 1994). Yet, it is interesting to note that the velocity of the P2-wave predicted by the new model ($\tau_W \neq 0$) is slightly higher than that predicted by the Biot's model in the high-frequency range. The reason for this phenomenon is that the effects of local fluid flow are considered in the new model and not in the Biot's model. At high frequencies very little local fluid flow can occur and the fluid trapped in the local heterogeneities such as grain microcracks and broken grain contacts move with the solid. This unrelaxed fluid within the local heterogeneities also makes the solid matrix more rigid with respect to the pore fluid. As demonstrated by Johnson et al. (1982), when the solid matrix is much more rigid than the pore fluid, the velocity of slow wave in the high-frequency range approaches $v_{p2} = v_W/\sqrt{T}$, where v_W is the velocity of compressional wave in the fluid and T is the tortuosity of the pores. The new model captures this increase in the velocity of the P2-wave at high frequencies due to the increase in the rigidity of the solid matrix caused by the unrelaxed pore fluid.

In practice, low-frequency acoustical measurements are difficult to obtain in rocks. Hence ultrasonic measurements (e.g., at $\omega > \omega_B$) are usually extrapolated to explain the low-frequency seismic behavior of porous media. Our numerical results, however, show that such an extrapolation must be done with caution.

8. Applications

Within the context of the proposed theory, relaxation time (τ_W) is the only parameter that stores the information on the details of local structure of porous media. It can be determined based on the measured

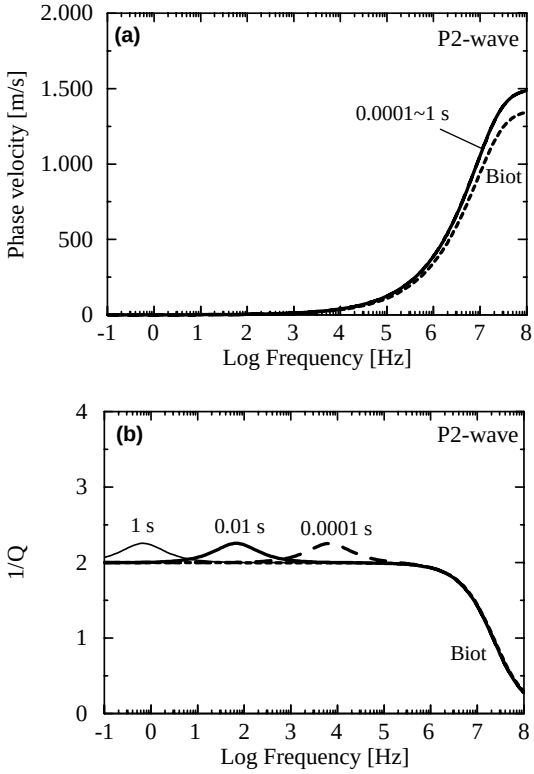

Fig. 4. Influence of the relaxation time (τ_W) on the velocity and attenuation of the P2-wave in a fully saturated D'Euville limestone.

seismic data. Such a feature endows the theory with great flexibility and capability in modeling the seismic behavior of fully saturated porous media.

8.1. Velocity dispersion and attenuation in Berea sandstone

Winkler (1985) measured the seismic response of Berea sandstone samples saturated by different fluids (brine and oil) and subjected to various confining pressures at a frequency of approximately 400 kHz. The properties of the solid and fluid constituents are directly obtained from Winkler (1985). The poroelastic parameters for various confining pressure are summarized in Tables 2 and 3. The *dry* velocities of the shear and compressional waves measured by Winkler are used to calculate the shear modulus G and K_D. The parameters α_B and B are estimated based on the magnitude of the measured velocity dispersion and the equations presented in Section 4.

The predicted pressure dependence of P1-wave velocity is compared with the measured values in Fig. 5. The velocities predicted by Biot's theory in the low-frequency limit and the high-frequency limit are also given in Fig. 5. In both brine-saturated and oil-saturated cases, Biot's theory underestimates the velocity. The discrepancy becomes smaller with an increasing confining pressure. The reason here is that, as the confining pressure increases, more and more microscopic apertures become closed and the effects of microscopic fluid flow are reduced. This phenomenon is an important feature of porous rocks containing microcracks or broken grain contacts (Mavko and Jizba, 1991). The values of the relaxation time (τ_W) are adjusted to match predictions with the measured data. The values of τ_W are given within the parentheses

Table 2
Poroelastic parameters of brine-saturated Berea sandstone

Parameter	Symbol	Confining pressure, MPa			
		5	10	20	40
Bulk modulus of matrix, GPa	K_D	8.32	10.78	13.26	15.18
Shear modulus of matrix, GPa	G	8.52	10.75	12.40	13.49
Effective stress coefficient	α_B	0.75	0.69	0.62	0.56
Pore pressure coefficient	B	0.54	0.44	0.36	0.30

Table 3
Poroelastic parameters of oil-saturated Berea sandstone

Parameter	Symbol	Confining pressure, MPa			
		5	10	20	40
Bulk modulus of matrix, GPa	K_D	8.30	11.21	14.10	15.76
Shear modulus of matrix, GPa	G	8.69	10.96	12.54	13.63
Effective stress coefficient	α_B	0.75	0.69	0.62	0.56
Pore pressure coefficient	B	0.48	0.38	0.30	0.25

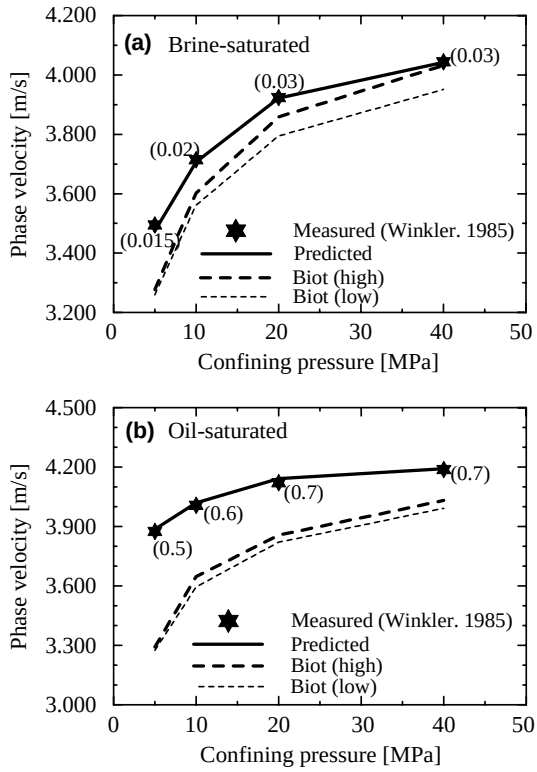

Fig. 5. Influence of the confining pressure on velocity of the P1-wave in fully saturated Berea sandstone: (a) brine-saturated; (b) oil-saturated. The numbers in parentheses represent the values of the relaxation time (τ_W) in 10^{-4} s. The measured data are obtained from Winkler (1985).

in Fig. 5. It can be seen that, in general, τ_W increases as the confining pressure increases. This can be explained using Eq. (61). When the confining pressure increases, α decreases and τ_W increases.

The predicted velocity dispersion of the P1-wave is described in Fig. 6. In both cases, the model predicts significant influence of confining pressure on the velocity dispersion due to microscopic (squirt) flow. The dispersion decreases with the increase in confining pressure and this can be attributed to the closure of microcracks and grain contacts. Interestingly, in the brine-saturated samples the measured data points are located in the frequency range between low and high limits, whereas in the oil-saturated samples the data points are in the high-frequency limit. Because all other material properties are quite similar for both types of samples, the difference is likely due to the viscosity η_W of the saturating fluids. The oil has a viscosity of 350 cp, which is two orders larger than that of brine (1 cp). As shown in Section 5, higher η_W (i.e., larger τ_W) shifts the characteristic frequency ω_L to a lower value.

The model predictions of the frequency dependence of attenuation are depicted in Fig. 7. When the confining pressure increases, the solid matrix becomes stiffer due to the closure of some of microcracks and grain contacts, resulting in decrease in the energy loss associated with the microscopic (squirt) fluid flow. It is quite clear that model correctly predicts this trend. Unfortunately, the measured data on the intrinsic attenuation (due to local fluid flow) are not available. By analyzing the total apparent attenuation and the scattering effects, Winkler (1985) suggested that, in contrast to those in the brine-saturated samples where much of the dispersive range lies above the measurement frequency (~400 kHz), the measured attenuations in the oil-saturated samples are obtained in the high-frequency tail of the relaxation. Our model predictions in Fig. 7 clearly justify this suggestion. This example shows that the proposed model can reasonably explain the acoustical response of porous rocks saturated with different types of fluids.

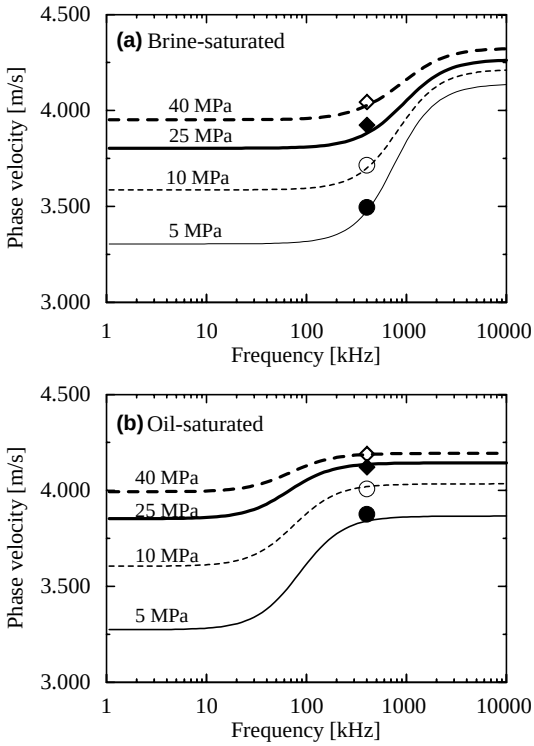

Fig. 6. Influence of the saturating fluid on velocity of the P1-wave in fully saturated Berea sandstone: (a) brine-saturated; (b) oil-saturated. The measured data are obtained from Winkler (1985).

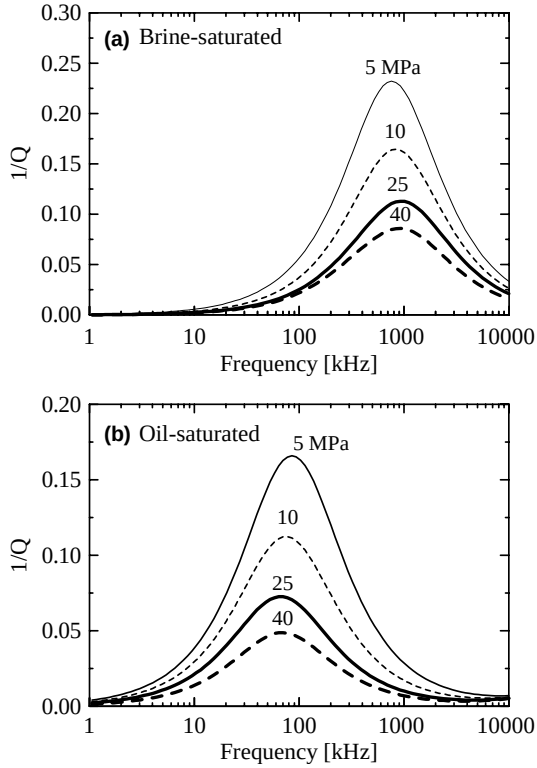

Fig. 7. Influence of the saturating fluid on attenuation of the P1-wave in fully saturated Berea sandstone: (a) brine-saturated; (b) oil saturated.

In practice, it is sometimes assumed that the operating frequency of microscopic (squirt) flow is in the high-frequency range. From this example, however, we should keep in mind that it is difficult to decide whether microscopic flow or mesoscopic flow dominates the energy loss merely based upon the characteristic frequency ω_L corresponding to local fluid flow. In some heavy-oil-bearing reservoirs, for instance, microscopic (squirt) flow could operate within the seismic frequencies.

8.2. Attenuation in D'Euville limestone

In this example, we shall calculate the attenuation based upon the measured velocity of the P1-wave in D'Euville limestone subjected to various confining pressures. The material properties are summarized in Table 1. The measured data on the velocity and attenuation are obtained from Lucet (1989) and presented in Fig. 8. These measurements were made in the seismic and ultrasonic frequencies.

From the measurements, we can see that there is significant velocity dispersion in the limestone under both confining pressures (3 and 5 MPa). The large magnitude of the measured attenuation implies that the energy loss could be attributed to local fluid flow. Indeed, the characteristic frequency ω_B of macroscopic flow is about 2 MHz, which is above the range of measurement frequencies. In order to determine the attenuation, we choose the value of τ_W such that the predicted velocities fit the measured data points. This yielded a value of $\tau_W \approx 1.2 \times 10^{-5}$ s for a confining pressure of 5 MPa, and $\tau_W \approx 8 \times 10^{-6}$ s for a confining pressure of 3 MPa. Note that the rock sample subjected to a larger confining pressure has a larger τ_W,

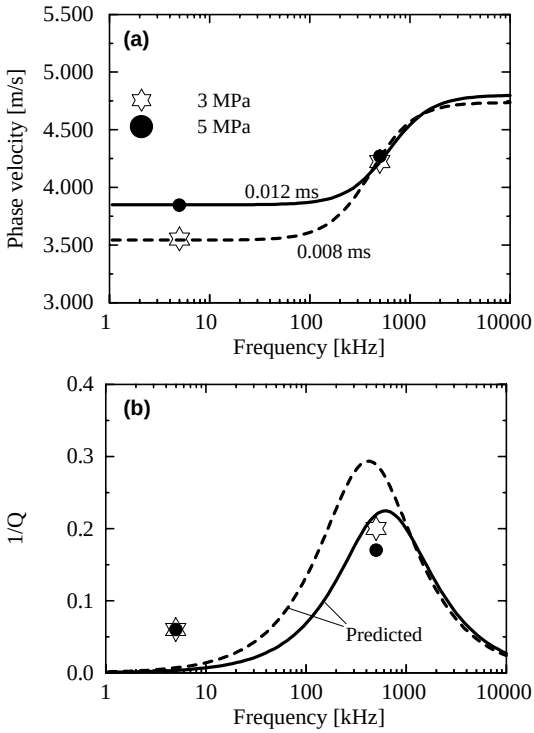

Fig. 8. (a) Velocity dispersion and (b) attenuation of the P1-wave in fully saturated D'Euville limestone at two different confining pressures. The measured data are obtained from Lucet (1989).

which is reasonable as explained in Section 8.1. In both cases, the magnitudes of predicted attenuations are comparable to the measured values, implying that the predicted results are reasonable.

In the above given calculations, no information on the details of the local structure are necessary. As shown the value of τ_W can be determined based on the measured seismic data. The value τ_W can be used to extract useful information about the local structure of the porous medium. If we assume that the microscopic apertures in the porous material are represented by cylindrical cavities, using Eq. (61), we can calculate the aspect ratio of these apertures as $\alpha = 2.4 \times 10^{-4}$ for 5 MPa, and $\alpha = 2.9 \times 10^{-4}$ for 3 MPa.

8.3. Effects of mesoscopic fluid flow

Several investigations in the laboratory have shown that significant dispersion and attenuation may occur at frequencies lower than 1 kHz (Spencer, 1981; Paffenholz and Burkhardt, 1989). It is believed that this phenomenon is due to radial fluid flow caused by the size limit of the samples, i.e., the so-called Biot–Gardner effect (Gardner, 1962; White, 1986). Because the sizes of the samples are much smaller than the wavelength and much larger than the pore size, the Biot–Gardner effect can be considered as some sort of mesoscopic fluid flow.

The frequency dependence of velocity dispersion and attenuation in the fully saturated Dolomite are shown in Fig. 9. The properties of Dolomite are summarized in Table 4. The data points are calculated from the measured Young modulus, Poisson ratio and attenuations of extensional and shear waves (Paffenholz and Burkhardt, 1989). The theoretical predictions (the solid line) agree very well with the experimental data for $\tau_W = 0.1$ s. Such a magnitude of τ_W excludes microscopic (squirt) flow from being the

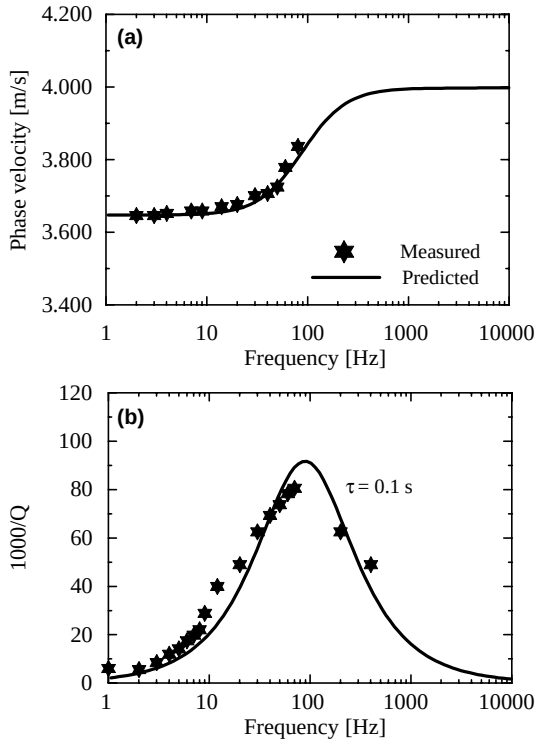

Fig. 9. (a) Velocity dispersion and (b) attenuation of the P1-wave in fully saturated Dolomite. The measured data (solid stars) are obtained from Paffenholz and Burkhardt (1989).

Table 4
Material properties of saturated Dolomite (Paffenholz and Burkhardt, 1989)

Parameter	Symbol	Value
Porosity	n	0.218
Bulk modulus of solid, GPa	K_S	37.0
Bulk modulus of water, GPa	K_W	2.25
Density of solid, kg/m^3	ρ^S	2833
Density of water, kg/m^3	ρ^W	1000
Viscosity of water, Pa s	η_W	0.001
Permeability, m^2	k	1.1×10^{-16}
Bulk modulus of matrix, GPa	K_D	13.7
Poisson ratio	v_D	0.18
Effective stress coefficient[a]	α_B	0.67
Pore pressure coefficient[a]	B	0.33

[a] α_B and B are estimated based on the equations presented in Section 4.

dominant loss mechanism, since the corresponding aspect ratio α ($\approx 2.6 \times 10^{-6}$) is too small for microscopic (squirt) flow to be significant (Jones, 1986). On the other hand, using Eq. (63), we estimate the characteristic length of mesoscopic flow as $\ell_m \approx 1.1$ cm, which is comparable to the diameter of the samples (5 cm). These calculations show that the new model can be used to describe the Biot–Gardner effect (Gardner, 1962; White, 1986).

8.4. Bulk attenuation in fully saturated Harz quartzite

It can be seen from Fig. 10 that there are two peaks in the frequency dependence of the bulk attenuation $Q_K(=\mathrm{im}(\widetilde{K}_U)/\mathrm{re}(\widetilde{K}_U))$ in the fully saturated Harz quartzite: one is at around 0.03 Hz, and the other is at 1.5 kHz. The data points are calculated from the measured attenuations Q_E^{-1} and Q_S^{-1} of extensional and shear waves (Paffenholz and Burkhardt, 1989). The model predicts that the peak at the lower frequency corresponds to $\tau_W \approx 250$ s, while at the higher frequency corresponds to $\tau_W \approx 2\times10^{-6}$ s. A simple calculation shows that the attenuation peak at high frequency can be attributed to microscopic (squirt) flow. Eq. (61) gives an estimate of aspect ratio of apertures as $\alpha \approx 6\times10^{-4}$. This value of aspect ratio is reasonable for low-porosity quartzite rocks. In contrast, the attenuation peak at 0.03 Hz must be induced by mesoscopic flow. Using (63) the characteristic length of mesoscopic heterogeneity can be calculated as $\ell_m \approx 12$ cm. This quantity is two times larger than the diameter (5 cm) of the specimens used in the experiment. Such a low-frequency attenuation peak can be attributed to the so-called Biot–Gardner–White effect that is induced by the mesoscopic fluid flow.

Attenuation measurements were recently performed over a broad range of frequencies at a single geological sequence of rocks (Sams et al., 1997). It was found that the peak of the frequency dependence of attenuation rests in the seismic frequency range. Pride et al. (2003) reanalyzed Sams et al.'s data and implied that the attenuation could be induced by mesoscopic flow. Unfortunately, the properties of relevant materials are not available. It is reasonable to expect the procedure proposed in this paper will also apply to Sams et al.'s data.

8.5. Summary and conclusions

When compressional waves propagate through porous media with local (either microscopic or mesoscopic) heterogeneities, internal pore fluid flow can take place at micro-, meso- and macro-scales. A linear dynamic model of fully saturated porous media with local heterogeneities is developed within the context of Biot's theory of poroelasticity, but based on volume averaging of microscopic equations. The effects of local fluid flow are taken into account by the notion of the dynamic compatibility condition on the interface between the solid material and the fluid.

Complex, frequency-dependent material properties, characterizing the viscoelastic behavior associated with local fluid flow, are derived. The complex material properties are obtained by determining the

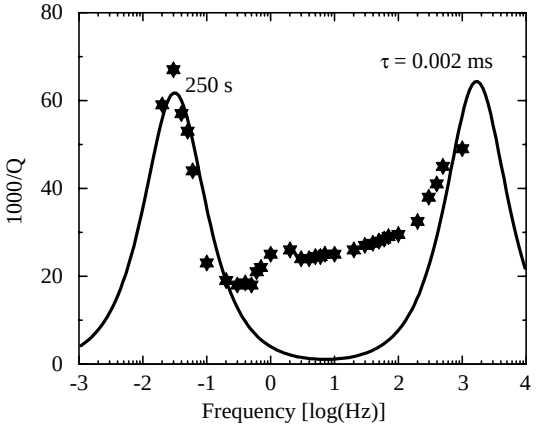

Fig. 10. Bulk attenuation Q_K^{-1} of the fully saturated Harz quartzite. Data points are calculated from the measured Q_E^{-1} and Q_S^{-1} (Paffenholz and Burkhardt, 1989).

quasi-static poroelastic parameters, the properties of individual constituents, and the relaxation time of the dynamic compatibility condition on the interface. In developing the relationships among various quasi-static poroelastic properties, we show that, as far as homogeneous porous materials are concerned, there are only three independent poroelastic parameters, and the effects of the local fluid flow on the viscoporoelastic behavior are negligible.

Theoretical predictions are compared with the measured acoustical data available in the literature. It is found that the model describes very well the acoustical behavior of porous media with local fluid flow over a wide range of frequencies. The proposed model provides a theoretical framework to simulate the acoustical behavior of fully saturated porous media without making any explicit assumption about the structure of local heterogeneities. The back calculated relaxation time of the dynamic compatibility condition on the interface can, however, provide insight into the nature of these local heterogeneities.

Acknowledgments

The authors are grateful to Dr. James G. Berryman of the Lawrence Livermore National Laboratory for providing the English translation of Gassmann's (1951) paper. Financial support for this work was provided by the US National Science Foundation under grants CMS-0112950 and CMS-0301457.

Appendix A. Relaxation time of microscopic fluid flow from a broken grain contact

When a compressional wave propagates through porous media, fluid flow takes place in microscopic apertures such as microcracks and broken grain contacts. Here microscopic apertures are treated as thin, open-edged cylindrical cavities (see Fig. 11), which can be viewed as the simple representations of broken contacts between solid grains. A typical cylindrical cavity has a diameter of 2ℓ and a thickness of $2h$, i.e., the aspect ratio $\alpha = h/\ell$. The total porosity n has two contributions: one is from the apertures and the other from the nearby pore space storing free fluid. In the notion of Dvorkin et al. (1995), the microscopic apertures are denoted as soft pores, with a porosity n_{so}, and the nearby pores are rigid pores, with a porosity n_{st}. It is assumed that $n_{so} \ll n_{st}$.

The derivation of the relaxation time of fluid pressure in microscopic apertures essentially follows the procedure by Leuer (1997) and originally proposed by Johnston et al. (1979). The fluid pressure p^W and the volume change of the fluid induced by a passing compressional wave are

$$p_{so}^{W} = -K_W\theta_{so}, \quad p_{ri}^{W} = -K_W\theta_{ri} \tag{A.1}$$

and

$$\Delta C_{so} = C_{so}\theta_{so}, \quad \Delta C_{ri} = C_{ri}\theta_{ri} \tag{A.2}$$

where K is the bulk modulus, θ is the dilation, and C is the volume concentration.

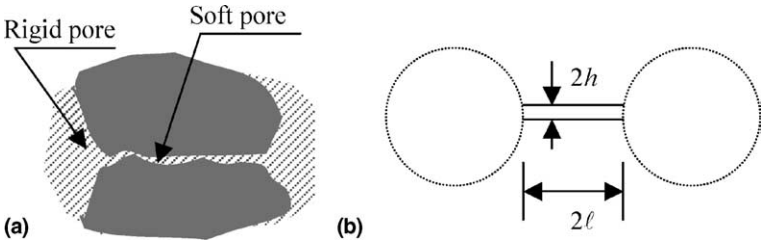

Fig. 11. Schematics of a broken grain contact in a porous medium: (a) broken grain contact; (b) geometric representation.

After the fluid pressure in the soft pores is totally relaxed, the fluid pressure will equilibrate between the soft pores and rigid pores. Let the equalized fluid pressures be $\bar{p}^{\mathrm{W}}$. The dilation of the fluid is $\bar{\theta} = -\bar{p}^{\mathrm{W}}/K_{\mathrm{W}}$. The total fluid volume displaced to equalize the pressure is given by

$$V_{\mathrm{t}} = \Delta\overline{C}_{\mathrm{so}} - \Delta C_{\mathrm{so}} = \Delta C_{\mathrm{ri}} - \Delta\overline{C}_{\mathrm{ri}} \tag{A.3}$$

where $\Delta\overline{C}_{\mathrm{so}} = C_{\mathrm{so}}\bar{\theta}$ and $\Delta\overline{C}_{\mathrm{ri}} = C_{\mathrm{ri}}\bar{\theta}$. It follows from (A.3) that

$$\bar{\theta} = \frac{\varepsilon\theta_{\mathrm{so}} + \theta_{\mathrm{ri}}}{1+\varepsilon} \tag{A.4}$$

where ε is the volumetric ratio of soft pores to rigid pore. Now, one obtains

$$V_{\mathrm{t}} = C_{\mathrm{so}}\frac{\theta_{\mathrm{ri}} - \theta_{\mathrm{so}}}{1+\varepsilon} \tag{A.5}$$

On the other hand, the average velocity w of the flow in the fluid layer between two plates separated by a small distance $2h$, induced by a pressure gradient $\mathrm{d}p/\mathrm{d}x$, is given by (Landau and Lifschitz, 1991)

$$w = \frac{h^2}{3\eta_{\mathrm{W}}}\frac{\mathrm{d}p}{\mathrm{d}x} \tag{A.6}$$

Hence, the flow rate of the fluid around the edge of the cavity is $q_0 = wA = (4\pi h\ell)w$. Setting $\mathrm{d}p/\mathrm{d}x \approx (p^{\mathrm{W}}_{\mathrm{so}} - p^{\mathrm{W}}_{\mathrm{ri}})/\ell$ and using (A.1), one obtains

$$q_0 \approx \frac{4\pi h^3 K_{\mathrm{W}}}{3\eta_{\mathrm{W}}}(\theta_{\mathrm{ri}} - \theta_{\mathrm{so}}) \tag{A.7}$$

Assuming the flow rate has a time dependence of $q_0\exp(-t/\tau_{\mathrm{W}})$, the total fluid volume displaced can be expressed by

$$V_{\mathrm{t}} = \int_0^\infty (q_0 \mathrm{e}^{-t/\tau_{\mathrm{W}}})\,\mathrm{d}t = q_0\tau_{\mathrm{W}} \tag{A.8}$$

Noting that $C_{\mathrm{so}} = 2\pi\ell^2 h$ and using (A.5) and (A.8), one derives

$$\tau_{\mathrm{W}} = \frac{3\eta_{\mathrm{W}}}{2K_{\mathrm{W}}\alpha^2(1+\varepsilon)} \tag{A.9}$$

Note that ε is a very small quantity, i.e. $\varepsilon \ll 1$. Hence, one obtains Eq. (61).

More realistically, microscopic apertures have a distribution of aspect ratio α_{m}. In this paper, for the sake of simplicity, we will not consider such a distribution. Instead, a typical single aspect ratio α is assumed for the apertures.

References

Berryman, J.G., 2002. Extension of poroelastic analysis to double-porosity materials: new technique in microgeomechanics. J. Eng. Mech. 128, 840–847.

Berryman, J.G., Thigpen, L., 1985. Linear dynamic poroelasticity with microstructure for partially saturated porous solids. J. Appl. Mech. 52, 345–350.

Biot, M.A., 1956a. Theory of propagation of elastic waves in a fluid-saturated porous solid. I. Low-frequency range. J. Acoust. Soc. Amer. 28, 168–178.

Biot, M.A., 1956b. Theory of propagation of elastic waves in a fluid-saturated porous solid. II. Higher frequency range. J. Acoust. Soc. Amer. 28, 179–191.

Biot, M.A., 1962. Generalized theory of acoustic propagation in porous dissipative media. J. Acoust. Soc. Amer. 34, 1254–1264.

Biot, M.A., Willis, D.G., 1957. The elastic coefficients of the theory of consolidation. J. Appl. Mech. 24, 594–601.

Brown, R.J.S., Korringa, J., 1975. On the dependence of the elastic properties of a porous rock on the compressibility of pore fluid. Geophysics 40, 608–616.
Cleary, M.P., 1978. Elastic and dynamic response regimes of fluid-impregnated solids with diverse microstructures. Int. J. Solids Struct. 14, 795–819.
Coussy, O., 1995. Mechanics of Porous Continua. Wiley, New York.
Dvorkin, J., Nur, A., 1993. Dynamic poroelasticity: a unified model with the squirt and the Biot mechanisms. Geophysics 58, 524–533.
Dvorkin, J., Mavko, G., Nur, A., 1995. Squirt flow in fully saturated rocks. Geophysics 60, 97–107.
Gardner, G.H.F., 1962. Extensional waves in fluid-saturated porous cylinders. J. Acoust. Soc. Amer. 34, 36–40.
Gassmann, F., 1951. Uber die elastizitat poroser medien. Vier. der Natur. Gesellschaft 96, 1–23.
Gist, G.A., 1994. Fluid effects on velocity and attenuation in sandstones. J. Acoust. Soc. Amer. 96, 1158–1173.
Gurevich, B., Zyrianov, V.B., Lopatnikov, S.L., 1997. Seismic attenuation in finely layered porous rocks: effects of fluid flow and scattering. Geophysics 62, 319–324.
Gurevich, B., Zadovnichaja, A.P., Lopatnikov, S.L., Shaoiro, S.A., 1998. Scattering of compressional waves in a fluid-saturated viscoelastic porous medium. Geophys. J. Int. 133, 91.
Hassanizadeh, M., Gray, W.G., 1979a. General conservation equations for multi-phase systems: 1. Averaging procedure. Adv. Water Res. 2, 131–144.
Hassanizadeh, M., Gray, W.G., 1979b. General conservation equations for multi-phase systems: 2. Mass, momentum, energy, and entropy. Adv. Water Res. 2, 191–203.
Johnston, D.H., Toksz, M.N., Timur, A., 1979. Attenuation of seismic waves in dry and saturated rocks: II. Mech. Geophys. 44, 691–711.
Johnson, D.L., Plona, T.J., Scala, C., Paseierb, F., Kojima, H., 1982. Tortuosity and acoustical slow wave. Phys. Rev. Lett. 49, 1840–1844.
Johnson, D.L., Koplik, J., Dashen, R., 1987. Theory of dynamic permeability and tortuosity in fluid-saturated porous media. J. Fluid Mech. 176, 379–402.
Jones, T.D., 1986. Pore fluids and frequency-dependent wave propagation in rocks. Geophysics 51, 1939–1953.
Klimentos, T., McCann, C., 1988. Why is the Biot slow compressional wave not observed in real rocks? Geophysics 53, 1605–1609.
Kümpel, H.-J., 1991. Poroelasticity: parameters reviewed. Geophysics 105, 783–799.
Lade, P.V., de Boer, R., 1997. The concept of effective stress for soil, concrete and rock. Geotechnique 47, 61–78.
Landau, L.D., Lifschitz, E.M., 1991. Lehrbuch der Theoretidchen Physik, Band IV: Hydraudynamik, 5. Aufl.: Akademie Verlag.
Leuer, K.C., 1997. Attenuation in fine-grained marine sediments: extension of the Biot–Stoll model by the "effective grain model" (EGM). Geophysics 62, 1465–1479.
Lucet, N., 1989. Vitesse et attenuation des ondes elastiques soniques et ultrasoniques dans les roches sous pression de confinement. Ph.D. thesis, The University of Paris.
Mavko, G., Jizba, D., 1991. Estimating grain-scale fluid effects on velocity dispersion in rocks. Geophysics 56, 1940–1949.
Mavko, G., Nur, A., 1975. Melt squirt in asthenosphere. J. Geophys. Res. 80, 1444–1448.
Mavko, G., Nur, A., 1979. Wave attenuation in partially saturated rocks. Geophysics 44, 161–178.
Muraleetharan, K.K., Wei, C., 1999. Dynamic behavior of unsaturated porous media: governing equations using the theory of mixtures with interfaces (TMI). Int. J. Numer. Anal. Meth. Geomech. 23, 1579–1608.
Murphy, W.F., Winkler, K.W., Kleinberg, R.L., 1986. Acoustic relaxation in sedimentary rocks: dependence on grain contacts and fluid saturation. Geophysics 51, 757–766.
Nur, A., Byerlee, J.D., 1971. An exact effective stress law for elastic deformation of rock with fluids. J. Geophys. Res. 76, 6414–6419.
O'Connell, R.J., Budiansky, B., 1977. Viscoelastic properties of fluid-saturated cracked solids. J. Geophys. Res. 82, 5719–5735.
Paffenholz, J., Burkhardt, H., 1989. Absorption and modulus measurements in the seismic frequency and strain range on partially saturated sedimentary rocks. J. Geophys. Res. 94, 9493–9507.
Pride, S.R., Berryman, J.G., 2003a. Linear dynamics of double-porosity dual-permeability materials: I. Governing equations and acoustic attenuation. Phys. Rev. E 68, 036603.
Pride, S.R., Berryman, J.G., 2003b. Linear dynamics of double-porosity dual-permeability materials: II Fluid transport equations. Phys. Rev. E 68, 036604.
Pride, S.R., Harris, J.M., Johnson, D.L., et al., 2003. Permeability dependence of seismic amplitudes. The Leading Edge 22, 518–525.
Pride, S.R., Berryman, J.G., Harris, J.M., 2004. Seismic attenuation due to wave-induced flow. J. Geophys. Res. 109, B01201.
Rice, J.M., Cleary, M.P., 1976. Some basic stress diffusion solutions for fluid-saturated elastic porous media with compressible components. Rev. Geophys. Space Phys. 14, 227–241.
Sams, M.S., Neep, J.P., Worthington, M.H., King, M.S., 1997. The measurements of velocity dispersion and frequency-dependent intrinsic attenuation in sedimentary rocks. Geophysics 62, 1456–1462.
Spencer Jr., J.M., 1981. Stress relaxation at low frequencies in fluid-saturated rocks: attenuation and modulus dispersion. J. Geophys. Res. 86, 1803–1812.

Wei, C., Muraleetharan, K.K., 2002a. A continuum theory of porous media saturated by multiple immiscible fluids: I. Linear poroelasticity. Int. J. Eng. Sci. 40, 1807–1833.

Wei, C., Muraleetharan, K.K., 2002b. A continuum theory of porous media saturated by multiple immiscible fluids: II. Lagrangian description and variational structure. Int. J. Eng. Sci. 40, 1835–1854.

White, J.E., 1986. Biot–Gardner theory of extensional waves in porous rods. Geophysics 51, 742–745.

Winkler, K.W., 1985. Dispersion analysis of velocity and attenuation in Berea sandstone. J. Geophys. Res. 90, 6793–6800.